#6064

International Symposium on Room Air Convection and Ventilation Effectiveness
University of Tokyo, July 22 – 24, 1992

# EXPERIMENTAL EVALUATION OF ROOM AIR AND AIR CONTAMINANT MOVEMENT

L.L. Christianson
Professor
University of Illinois
Urbana, Illinois, U.S.A.

J.S. Zhang
Research Associate
National Research Council
Ottawa, Ontario, Canada

G.J. Wu
Assistant Professor
University of Wisconsin
Madison, Wisconsin, U.S.A.

## ABSTRACT

A Room Ventilation Simulator has been developed with several unique features: an outer room with a HVAC (Heating Ventilating and Air-Conditioning) system to simulate different weather conditions by controlling the ambient air environment around the test room; an inner test room of modular design to facilitate changing room dimensions and configurations; an independent HVAC system for the inner test room to study different air supplies; an air delivery system capable of providing air flow rates of 2 to 52 air changes per hour; a uniform floor heating system of 48 individually controllable panels to simulate internal heat loads; a computer controlled data acquisition and probe positioning system to allow automatic measurements at precisely positioned locations; and a flow visualization system to record room air and contaminant flow patterns.

In this paper experimental results are described from a full scale test room (5.49×7.32×2.44 m) including the spatial distributions of mean velocity, turbulence intensity, kinetic energy of turbulence, temperature and contaminant concentrations. Discussions focus on the effects of the diffuser air velocities and internal heat loads on the air flow characteristics. The detailed experimental data are also useful for evaluating and improving numerical simulation models of room air and air contaminant motions.

## KEYWORDS

Ventilation, Flow Behaviour, Turbulence, Air Distribution

## INTRODUCTION

Understanding room air distribution is essential to the design of ventilation systems and control of room thermal and air quality conditions. Air velocities in occupied zones of a room directly affect the thermal comfort of occupants. The movement of air within a room also affects the release rate of heat and contaminants from sources, determines how the heat and contaminants distribute, and thus affects the air quality available to the occupants. In addition, proper air distribution can reduce the ventilation rate necessary for removing air contaminants and moisture, and thus reduce building energy consumption. Study of room air distribution is important to many applications including commercial and residential rooms, clean room manufacturing, electronic and computer rooms, biomedical research, hospital disease control, and greenhouse and animal agriculture (Christianson 1989).

Room air and air contaminant distribution is a complicated process. Researchers have developed

a limited understanding through experimental measurements (e.g., Straub and Chen 1957, Baturin 1972, Miller and Nevins 1972, Nielsen et al. 1978, Randall and Battams 1979, Timmons 1984, Sandberg 1989, and Zhang et al. 1990) and numerical modelling (e.g., Nielsen et al. 1979, Baker and Kelso 1989, Murakami and Kato 1989, Chen and Jiang 1991, and Whittle and Clancy 1991). Research efforts have concentrated on high ventilation rate conditions (fully turbulent flow), isothermal conditions (no internal heat loads), limited if any internal obstructions (no furniture and equipment), and simple room geometries to simplify the problem. Realistic room ventilation flow usually has multi-flow features, including high and low turbulence, which increases the complexity of both physical and mathematical modelling. Physical modelling is also complicated by the difficulty of air velocity measurements since low air velocities (<50 ft/min) are involved.

Methods commonly used for investigating room air and air contaminant distribution are full scale measurements, similitude model study and numerical simulations. Measurements in full scale rooms are essential to the understanding of room flow behaviour and the evaluations of indirect techniques such as similitude studies and numerical models, and currently are the only assured method of evaluating room airflow. However, it is generally expensive and inconvenient to conduct full scale experiments, and the results can only be applied to the rooms that are identical (at least very similar) to the prototype studied.

Similitude study involves experiments in a reduced scale model room and extrapolations of the results from this model room to its prototype. More importantly, similitude makes it possible to extrapolate experimental findings to a variety of rooms with similar geometry without the need for physical modelling of every prototype. The application of similitude to room air flow is limited by our knowledge of proper scaling methods for extrapolating the data. Knowledge of the regional characteristics of the room air flow, including its turbulent behaviour, is necessary to the development of the scaling theory.

Numerical simulation involves mathematically modelling the room airflow and numerically solving the model. While complicated, it is in principle the most generalized method and thus most convenient for predicting room air flows. However, advances in numerical modelling are limited by the lack of compatible, adequately detailed experimental data for model evaluation, and by the lack of knowledge of the room air flow characteristics, especially the turbulent flow features.

The objectives of this research were to improve the understanding of the mean and turbulent behaviour of realistic room ventilation flows and provide experimental data for evaluating and improving numerical simulation models of room air motion.

## EXPERIMENTAL FACILITY AND PROCEDURE

To investigate the various aspects of room air distribution, a Room Ventilation Simulator (Figure 1) was developed with several unique features: an outer room with an HVAC (Heating Ventilating and Air-Conditioning) system to simulate different weather conditions by controlling the ambient air environment around the test room; an inner test room of modular design to facilitate changing room dimensions and configurations; an independent HVAC system for the inner test room to study different air supplies; an air delivery system capable of providing air flow rates of 2 to 52 air changes per hour; a uniform floor heating system of 48 controllable panels to simulate internal heat loads; a computer controlled data acquisition and probe positioning system to allow automatic measurements at precisely positioned locations; and a flow visualization system to record room air flow patterns. Additionally, computer software was developed for data analyses. Details can be found in Wu et al. (1990), Zhang (1991) and Zhang et al. (1992).

Results presented in this paper are from a full scale experimental-set up show in Figure 2. The test room has a continuous slot diffuser and a continuous slot exhaust. Measurements indicated that the flow inside the room was practically two dimensional except very close to the two end walls (Zhang

1991). The internal heat load was simulated with the heating panels uniformly distributed on the floor surface.

Velocities and temperatures were measured at 205 locations at the central section of the room with hot wire anemometer and thermocouple, respectively. The measurement grid was non-uniform with more locations measured in the diffuser jet region and over the floor surface where relatively high velocity gradient was expected. Additionally, smoke generated by titanium tetrachloride was used to visualize the room airflow patterns. Test conditions are listed in Table 1.

**TABLE 1 Test Conditions**

| Test | $U_d$ (m/s) | $T_d$ (°C) | $T_e$ (°C) | $T_f$ (°C) | $\Delta T_{fd}$ (°C) | $Re_d$ | $Ar_{fd}$ | Q (ACH) |
|---|---|---|---|---|---|---|---|---|
| P1 | 2.54 | 23.9 | 23.9 | 23.9 | 0 | 8193 | 0 | 27.9 |
| P2 | 1.78 | 23.9 | 23.9 | 23.9 | 0 | 5735 | 0 | 19.5 |
| P3 | 0.76 | 23.9 | 23.9 | 23.9 | 0 | 2458 | 0 | 8.6 |
| P4 | 1.78 | 24.1 | 32.4 | 61.5 | 37.4 | 5735 | 0.0186 | 19.5 |
| P5 | 1.78 | 23.3 | 28.9 | 49.9 | 26.6 | 5735 | 0.0135 | 19.5 |
| P6 | 1.78 | 23.1 | 26.7 | 39.7 | 16.4 | 5735 | 0.0085 | 19.5 |

* $w_d$=2 inch for all the tests.

## RESULTS AND DISCUSSION

### Flow Patterns

The common flow behaviour among the six test cases (Figures 3 through 8) is that the incoming air attached to the ceiling after entering the room because of the Coanda effect. The air then travelled along the ceiling for a certain distance (called attachment length) until it separated from the ceiling or reached the opposite wall. Air below the jet was entrained by the jet so that a reverse flow formed below the jet. However, there were substantial differences among the six tests, which resulted from different diffuser air velocities and thermal buoyancy effects caused by the internal heat loads.

Effect of Diffuser Air Velocity. At the highest diffuser air velocity (Figure 3), there was a strong primary recirculation eddy in the upper right corner and a secondary recirculation eddy in the lower left corner.

The flow pattern in the medium diffuser air velocity test (Figure 4) was very similar to that from the highest diffuser air velocity case, but the secondary eddy at the lower left corner was not clearly observed in the medium velocity case. This may be explained by the reduced inertial effect due to the decrease in the diffuser air velocity. The momentum in the reverse flow was not enough to generate the strong secondary eddy in the lower left corner.

At the lowest diffuser velocity (Figure 5), the reverse flow below the diffuser jet occupied only a small upper portion of the flow field. This was again due to the small amount of momentum in the diffuser air jet which resulted in much less entrained air. There appeared to be a large weak recirculation flow in the lower portion of the flow field due to molecular viscosity, but the flow there was essentially stagnant.

Effect of Thermal Buoyancy. For a lower internal heat load, the diffuser air jet attached to the

ceiling for a longer distance before it separated from the ceiling. Therefore, the effect of the thermal buoyancy was to pull the diffuser air toward the floor. This was expected because the incoming air had a lower temperature than the room air. The separation point of the diffuser air jet would depend on the balance between the Coanda effect (or inertial effect) and the thermal buoyancy effect. The Coanda effect is dependent on the air velocities within the jet, which represents the inertial effect. As the air velocities within the jet decay along the trajectory of the jet, the Coanda effect becomes smaller and smaller. The jet would start to separate from the ceiling surface when the Coanda effect is equal to the thermal buoyancy effect. The Archimedes number represents the ratio between the thermal buoyancy and inertial effects and is therefore naturally used to characterize the room air flow patterns.

It was also observed that flow in the non-isothermal cases had stronger random behaviour, compared to the isothermal cases. For the non-isothermal cases, flow observed at the same location but different times had more directional variations.

**Statistical Characteristics**

The room air flow involves turbulence. The movement of fluid elements in a turbulent flow field has a strong random feature. Statistical analysis of the air velocity signals within the room is a fundamental step toward the understanding of the flow behaviour.

Features of the Velocity. As shown in Figures 9 and 10, the velocity signals had strong random features. The air velocities in the jet regions contained more high frequency fluctuations and were more turbulent compared to those in the occupied regions. A higher diffuser air velocity resulted in more turbulent flow in the occupied regions. For the same diffuser air velocity, the heat generated from the floor was found to cause more fluctuations in the velocity signals of the occupied region (Zhang 1991), indicating the contribution of the thermal buoyancy to the generation of turbulence in the occupied region.

Probability Density Function. Probability density functions are shown for test P3 (Figure 11). The random fluctuation of air velocity at a fixed point followed the normal distribution in general for both isothermal and non-isothermal flows, although the latter was noted to follow the normal distribution more closely. Therefore, one can use measured mean velocity and standard deviation to determine the velocity range at the measured point for a given confidence level. This agreed with the field measurement results of Thorshauge (1982). Such information is useful for assessing the thermal comfort in ventilated buildings because one needs to know the percentage of time when air velocities in the occupied regions satisfy the given criterion.

The histograms of velocity fluctuations (Figure 11) are skewed slightly to the right. This may be caused by the limitation of the hot wire anemometer which is unable to detect the reverse flow. In other words, the negative velocities (i.e., air velocities in the negative direction) is sensed as positive values by the hot wire anemometer. As a result, the histograms of velocity fluctuations are right-skewed since the negative velocities are folded to the right.

Energy Spectral Density Function. The energy spectral density function E(f) is defined as

$$\int_0^{+\infty} E(f)\,df = (u')^2 \qquad (1)$$

where, $(u')^2$ is the variance representing the total energy of the velocity fluctuation. E(f) represents the distribution of the kinetic energy of turbulence fluctuations over different frequency components. The higher frequency components correspond to smaller eddies and the lower to larger eddies.

Velocities in the jet region contained higher levels of kinetic energy of turbulence as compared to the occupied regions, especially for the low diffuser velocity case (Figures 12 and 13). The distribution also extended to higher frequencies for the jet regions. The large velocity gradients in the

jet regions were mainly responsible for the generation of the turbulence according to the turbulence theory (Hinze 1975). High velocity gradients also generated more small eddies which corresponded to the high frequency fluctuations.

It was also noted that thermal buoyancy due to the heat production from the floor increased the turbulence energy in the occupied region, but had little effect on the turbulent kinetic energy in the jet region. Therefore, the contribution of thermal buoyancy to the turbulence production within the room is limited in the occupied region which is close to the heat sources (floor surfaces in this case).

**Mean Velocity**

Spatial distributions of mean velocity is shown in Figure 14[1], where all velocities are made dimensionless by dividing by the diffuser air velocity. The trajectory of the diffuser air jet can be traced by following the location at which the maximum velocity occurred in each measurement column (x/W). A common feature for all the tests was that the incoming air jet bent toward the ceiling after entering the room. It then travelled along the ceiling for a certain distance before separating from the ceiling again. This agrees with the flow patterns discussed earlier.

In the region where the jet attached to the ceiling, the measured velocity profiles were similar to a "wall jet" type flow. Conventional "wall jet" theories (Schlichting, 1979) may be tested with the present data to evaluate whether they adequately describe this region or modifications are necessary for acceptably accurate predictions.

The velocity profiles close to the floor ($y/H > .75$) did not show similarity with the "wall jet" type flow, but were more or less uniform. With a higher diffuser air velocity (i.e., a higher $Re_d$) than the case studied, a higher remaining momentum from the diffuser air jet would be available to the reverse flow. Due to the surface effect, a "wall jet" type flow would also be produced in the regions close to the floor, as reported by Jin and Ogilvie (1990). This is an important difference between high and low ventilation rate flows (i.e., between high and low $Re_d$).

**TABLE 2 Dependence of average velocity in the occupied region[2] on the Reynolds number**

| $U_d$, m/s | $Re_d$ | U, m/s | $U/U_d$ | Test |
|---|---|---|---|---|
| 0.76 | 2458 | 0.08 | 0.108 | P3 |
| 1.78 | 5489 | 0.14 | 0.077 | P2 |
| 2.54 | 8192 | 0.18 | 0.070 | P1 |

The average velocity in the occupied region increased with the $Re_d$ as expected, but the dimensionless average velocity ($U/U_d$) decreased (Table 2). This again indicates the dependence of the air distribution on the Reynolds number. The decrease of the dimensionless average velocity ($U/U_d$) may be explained by the increased degree of turbulent mixing when the Reynolds number increased. This is

[1] Spatial distributions of mean velocities, turbulence intensities, turbulent kinetic energy and temperatures are presented only for test P6 only due to the page limit. Data for the other tests can be found in Zhang (1991).

[2] The occupied region is defined as the space from the floor to 6 ft high level and 1 ft from each side walls, which corresponds to $0.25 < y/H < 1.0$ and $0.56 < x/W < 0.94$, respectively.

in agreement with the previous experimental results in a 1/12th scale model (Zhang et al., 1990). Other researchers (e.g., Timmons, 1979) showed that when the Reynolds number was larger than a threshold, the distribution of mean air velocity within a ventilated room became independent of the Reynolds number and the threshold value increased with the room scale. However, most realistic room ventilation flows have Reynolds numbers well below the threshold as in the present study. Therefore, the dependence of room air flows on the Reynolds number has to be considered in the study of realistic room ventilation flows.

Increasing thermal buoyancy effect decreased the distance at which the air jet travelled along the ceiling and also made the jet expand faster. When the jet fell, it produced a region with relatively high air velocities in some part of the occupied region.

The average velocity in the occupied region was higher in the non-isothermal case than in isothermal case since the diffuser air jet dropped directly to the occupied region (Table 3). However, for the three non-isothermal test cases, the average velocity in the occupied region decreased with the increase of internal heat load and hence the Archimedes number. When the internal heat load increased, turbulent mixing due to thermal buoyancy increased, resulting in a higher velocity decay in the diffuser air jet and thus a lower mean air velocity in the occupied zone.

**TABLE 3 Dependence of average velocity in the occupied region[4] on the Archimedes number**

| $\Delta T_{fd}$, °C | $Ar_{fd}$ | U, m/s | $U/U_d$ | Test |
|---|---|---|---|---|
| 0.0 | 0.0 | 0.14 | 0.077 | P2 |
| 16.4 | 0.0085 | 0.18 | 0.101 | P6 |
| 26.6 | 0.0135 | 0.17 | 0.098 | P5 |
| 37.4 | 0.0186 | 0.15 | 0.084 | P4 |

**Turbulence Intensity**

The turbulence intensity is defined as the ratio between standard deviation (u') of velocity fluctuations and the mean velocity (U). It represents the degree of turbulence at a local point. The distribution patterns of the turbulence intensity within the test room were not as apparent as in mean velocity distribution (Figure 15). In general, relatively high values were distributed in the intermittent region at the edge of the diffuser air jet and at the central region of the recirculation eddy.

The average turbulence intensity in the occupied region increased with the increase of the diffuser air velocity as expected (Table 4). It also increased with the internal heat load because the thermal buoyancy caused the diffuser jet to drop into the occupied region and also contributed to the production of turbulence within the occupied region.

**Turbulent Kinetic Energy**

The kinetic energy of turbulence (k) is defined as $0.5u'^2$. It is a more appropriate term to represent the importance of turbulence effect on the room air motion than turbulence intensity. The kinetic energy of turbulence in the diffuser jet region was substantially larger than in the occupied region (Figure 16), especially in the isothermal tests. Since the magnitude of turbulent kinetic energy in a local region depends on the turbulence generated within the region and that transported from upstream, one may infer that the turbulence within the room was mainly generated in the diffuser jet region due to the strong interaction between the incoming air and the room air, and between the jet and the ceiling surface.

TABLE 4 Average turbulence intensity in the occupied region[4]

| $U_d$, m/s | $Re_d$ | $\Delta T_{fd}$, °C | $Ar_{fd}$ | u'/U, % | Test |
|---|---|---|---|---|---|
| 0.76 | 2458 | 0 | 0 | 6.5 | P3 |
| 1.78 | 5489 | 0 | 0 | 23.6 | P2 |
| 2.54 | 8192 | 0 | 0 | 27.9 | P1 |
| 1.78 | 5489 | 16.4 | 0.0085 | 26.1 | P6 |
| 1.78 | 5489 | 26.6 | 0.0135 | 29.9 | P5 |
| 1.78 | 5489 | 37.4 | 0.0186 | 33.9 | P4 |

generated turbulence was then transported to the other parts of the room. In the transport process, the velocity fluctuations were also damped by viscous effects, resulting in lower turbulent kinetic energy in the occupied region. This phenomenon agrees with the turbulence theory (Hinze 1975), since large mean velocity gradients were present in the jet region, but not in the occupied region.

The non-dimensionalized turbulent kinetic energy of the occupied region was larger in the case of a higher diffuser velocity (Table 5). If the diffuser air velocity increases further, a sufficiently high velocity gradient may be present between the solid surfaces of the opposite wall and the floor and the adjacent flow, resulting in significant turbulence production, and thereby increasing the turbulent kinetic energy in the occupied region significantly. However, most realistic ventilation flows have low velocities (<50 fpm) over the floor surface so that such additional turbulence production is negligible as compared to the turbulence production in the jet region.

The average turbulent kinetic energy of the occupied region in non-isothermal flows was approximately 115% larger than in the isothermal flows (Table 5). This was again partly due to the contribution of thermal buoyancy to the turbulence production, especially within the occupied region itself, and partly due to the drop of the diffuser jet into the occupied region.

TABLE 5 Average Kinetic Energy of Turbulence in the Occupied Region[4]

| $U_d$, m/s | $Re_d$ | $\Delta T_{fd}$, °C | $Ar_{fd}$ | $k/(0.5U_d)^2$ | Test |
|---|---|---|---|---|---|
| 0.76 | 2458 | 0 | 0 | 0.00009 | P3 |
| 1.78 | 5489 | 0 | 0 | 0.00042 | P2 |
| 2.54 | 8192 | 0 | 0 | 0.00044 | P1 |
| 1.78 | 5489 | 16.4 | 0.0085 | 0.00082 | P6 |
| 1.78 | 5489 | 26.6 | 0.0135 | 0.00098 | P5 |
| 1.78 | 5489 | 37.4 | 0.0186 | 0.00092 | P4 |

## Mean Temperature

The distribution of mean temperature for the non-isothermal tests conducted were mainly

determined by the mean velocity distribution (Figure 17). In other words, the temperature was lower upstream of the flow. As the air travelled, it was heated by the adjacent warmer air through turbulent mixing and molecular diffusion.

In the occupied region, the room air temperatures were much more uniform than the mean velocity distribution. This is mainly because the temperature field had a different boundary conditions from the velocity field. Temperatures on the surfaces of walls, ceiling and floor were higher than (on the floor surface) or equal to (on other surfaces assuming adiabatic condition) the temperature of the air attached to the surfaces, while the air velocities on these surfaces were zero due to the air viscosity. Additionally, the molecular heat diffusion was faster than the molecular momentum diffusion since the Prandtl number of the air is about 0.7. The Prandtl number represents the ratio between the momentum and thermal diffusion rates due to molecular motion (Kays and Crawford, 1980).

**Velocity Characteristics at the Diffuser**

As shown in Figure 19, the mean velocity profile at the diffuser was not uniform. Neither was the turbulent kinetic energy. Numerical modellers usually assumed a uniform turbulence intensity between 4% and 5% (e.g., Murakami, 1991). This would be appropriate only for the central part of the diffuser. The measured profile of turbulence intensity showed higher values (up to 75%) at the edges of diffuser opening (Figure 20). Since the diffuser air jet has a dominating effect on the room air movement, it is expected that numerical simulations of room air distribution are very sensitive to the velocity and turbulence conditions at the diffuser. Therefore, measured profiles of mean velocity and turbulence intensity at the diffuser are essential for evaluating numerical simulation models of room air distribution.

## SUMMARY AND CONCLUSIONS

A unique Room Ventilation Simulator is developed to study the various aspects of room air and air contaminant distributions. Experiments with a $5.49 \times 7.32 \times 2.44$ m full scale test room indicated:

1. Turbulence of room ventilation flows is mainly generated by the diffuser air jet. The turbulent kinetic energy in the occupied regions is significantly smaller and distributed in a lower frequency range as compared to the diffuser jet region.
2. Normal distribution can be used to approximate the velocity fluctuations in the room ventilation flow.
3. Air distribution in realistic isothermal ventilation flows is Reynolds number dependent. Increasing the Reynolds number ($Re_d$) decreases the dimensionless average velocity ($U/U_d$) and increases the turbulent kinetic energy and turbulence intensity in the occupied region.
4. The internal heat load may have significant effects on the room air distribution, causing the diffuser air jet to fall more quickly after entering the room. This causes a higher spatial average of mean velocity in the occupied region for the non-isothermal cases as compared to the isothermal case under the same diffuser air velocity. The thermal buoyancy also contributes to the turbulence production within the room and thereby increases the turbulent kinetic energy and turbulence intensity in the occupied region.
5. The measured velocity and turbulent kinetic energy profiles at the diffuser were nonuniform. The measured turbulence intensity at the diffuser edges was significantly higher than 4-5% as used in many numerical simulations of room air motion.

## NOMENCLATURE

ACH = Air changes per hour;

$Ar_{fd}$ = Archimedes number defined as $\frac{\beta g w_d (T_f - T_d)}{U_d^2}$;

E(f) = Spectral density function of velocity fluctuations, $(m/s)^2$;

f = Frequency, Hz;

g = Gravitational acceleration rate, $m/s^2$;

H = Room height, m;

k = Turbulent kinetic energy, $(m/s)^2$;

L = Length of the room (in Z direction), m;

$l_d$ = Length of the diffuser slot (in Z direction), m;

Q = Ventilation rate, $m^3/s$;

Re = Reynolds number defined as $\frac{U_d w_d}{\nu}$;

$T_f$ = Maximum temperature in room (e.g., on the heated surface), °C;

$T_d$ = Diffuser air temperature °C;

$T_e$ = Air temperature at the exhaust, °C;

$\Delta T_{ed}$ = $T_e - T_d$, °C;

$\Delta T_{fd}$ = $T_f - T_d$, °C;

u′ = Standard deviation of velocity, m/s;

$U_d$ = reference velocity, diffuser velocity at the measurement plane (z=0), m/s;

W = Width of the test room (in X direction), m;

$w_d$ = Width of the diffuser slot (in Y direction), m;

$w_e$ = Slot width of the exhaust, m;

x, y, z = Eulerian Cartesian coordinates, m;

$y_d$ = Distance from the ceiling to the diffuser upper edge, m;

$y_e$ = Distance from the ceiling to the upper edge of the exhaust, m;

$\alpha$ = Thermal diffusion coefficient, $m^2/s$;

$\beta$ = Thermal expansion coefficient, 1/K;

$\nu$ = Kinematic viscosity, $m^2/s$;

$\rho$ = Density of diffuser air, $kg/m^3$;

## REFERENCES


Baturin, V.V. 1972. Fundamentals of Industrial Ventilation. 3rd edition. Pergamon Press, Oxford, U.K.

Christianson, L.L. 1989. Building Systems: Room Air and Air Contaminant Distribution, ASHRAE, Atlanta, GA.

Hinze, J.O. 1975. Turbulence. McGraw-Hill, Inc., New York, NY.

Jin, Y. and J.R. Ogilvie. 1990. Near floor air speeds from center slot air inlets in swine barns. ASAE Paper No. 904004. American Society of Agricultural Engineers, St. Joseph, MI.

Kays, W.M. and M.E. Crawford. 1980. Convective Heat and Mass Transfer. McGraw-Hill, Inc., New York, NY.

Miller, P.L. and R.G. Nevins. 1972. An analysis of performance of air distribution systems. Transactions of ASHRAE 78(2):191.

Murakami, S. and S. Kato. 1989. Current status of numerical and experimental methods for analyzing flow field and diffusion field in a room. In Building Systems: Room Air and Air Contaminant Distribution, ed. L.L. Christianson, 621-642.

Nevins, R.G and P.L. Miller. 1972. Analysis, evaluation and comparison of room air distribution performance - a summary. Transactions of ASHRAE 78(2):235-242.

Randall, J.M. and V.A. Battams. 1979. Stability criteria for airflow patterns in livestock buildings. J. Agric. Engng Res. 24(3):361-374.

Sandberg, M. 1989. Velocity characteristics in mechanically ventilated office rooms. In Room Vent '87, Proc. 1st international conference of air distribution in ventilated spaces, Session 2A, Stockholm, Sweden, 10-12 June.

Schlichting, H. 1979. Boundary-Layer Theory. McGraw-Hill, Inc., New York, NY.

Straub, H.E. and Chen, M.M. 1957. Distribution of air within a room for year-round air-conditioning - part II. University of Illinois Engineering Experiment Station Bulletin, No. 442. University of Illinois, Urbana, IL.

Timmons, M.B. 1984. Use of physical models to predict the fluid motion in slot-ventilated livestock structures. Transactions of ASAE 27(2):502-507.

Whittle, G.E. and E.M. Clancy. 1991. Evaluation of cases B,D,E - presentation of results from measurements and simulations. IEA Annex 20 Research Report No. 1.22.

Wu, G.J., L.L. Christianson, J.S. Zhang and G.L. Riskowski. 1990. Adjustable room ventilation simulator for room air and air contaminant distribution modelling. In Indoor Air '90, Proc. 5th international conference on indoor air quality and climate, 4:237-242.

Zhang, J.S., L.L. Christianson and G.L. Riskowski. 1990. Regional air flow characteristics in a mechanically ventilated room under non-isothermal conditions. Transactions of ASHRAE 95(2).

Zhang, J.S., L.L. Christianson, G.J. Wu and G.L. Riskowski. 1991. An Fundamental Study of Two Dimensional Room Ventilation Flows under Isothermal and Non-isothermal Conditions. PhD Thesis, University of Illinois at Urbana-Champaign, Urbana, IL.

Zhang, J.S., G.J. Wu and L.L. Christianson. 1992. Detailed measurements of room air distribution for evaluating numerical simulation models. ASHRAE Technical Paper No. 3548, Anaheim, January.

## ACKNOWLEDGEMENT

This study was sponsored by the U.S. National Science Foundation and University of Illinois Campus Research Board. Their financial support is highly appreciated. Authors are also grateful for the help of Jolien de Vos, Steve Ford and Bo Zhang in conducting the experiments.

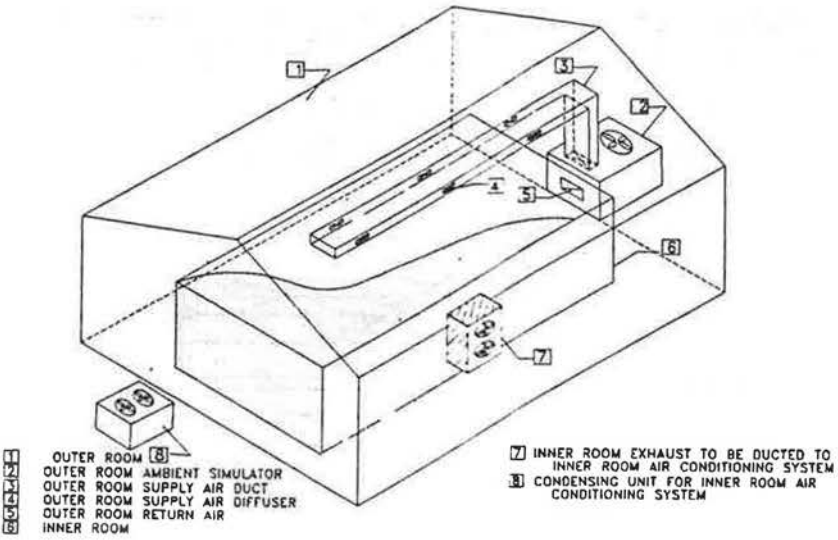


**Figure 1** Schematic of the Room Ventilation Simulator

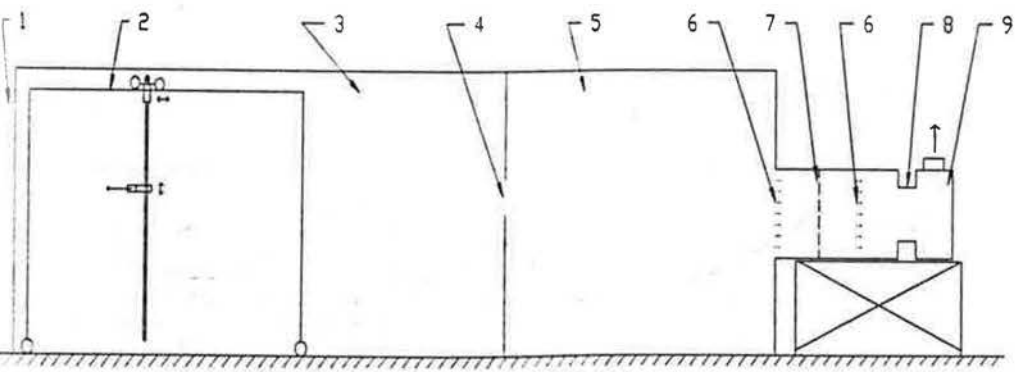


1 Continuous slot diffuser
2 Probe traverse unit
3 Test room
4 Continuous slot exhaust
5 Exhaust plenum
6 Flow settling screens
7 Perforated plate
8 Flexible connector
9 Centrifugal fan

**Figure 2** Experimental set up for the full scale room
(z direction is into the page)

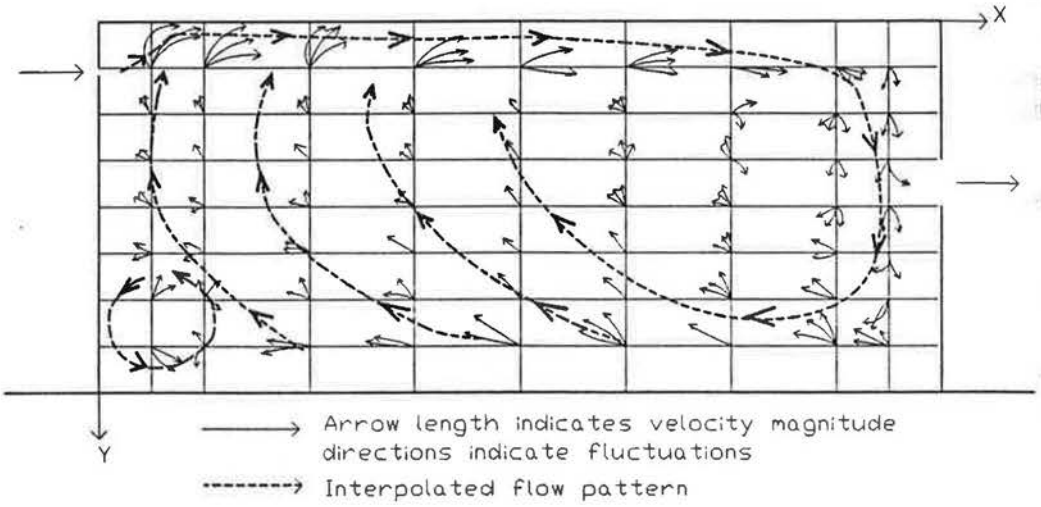


**Figure 3** Flow pattern of test P1: $U_d$=2.54 m/s, $\Delta T_{fd}$=0 °C

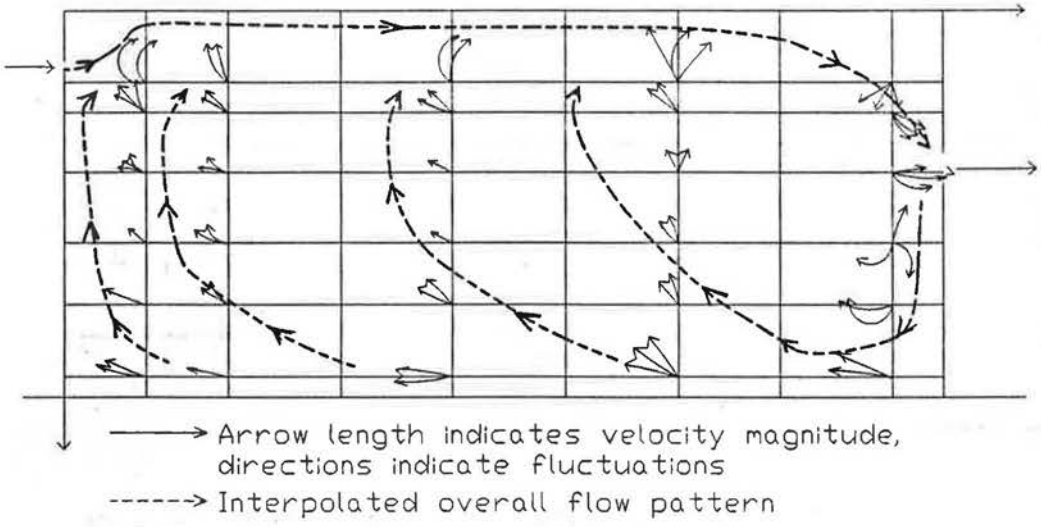


**Figure 4** Flow pattern of test P2: $U_d$=1.78 m/s, $\Delta T_{fd}$=0 °C

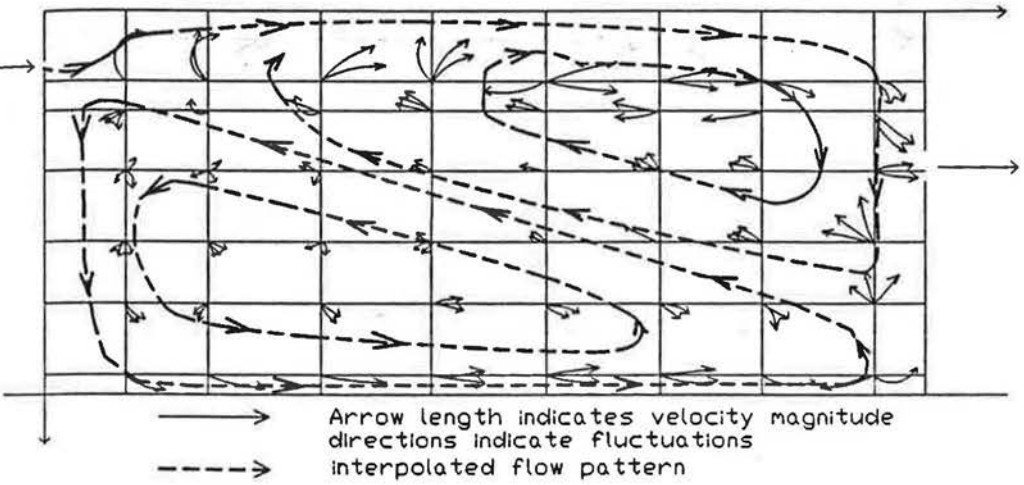


**Figure 5** Flow pattern of test P3: $U_d$=0.76 m/s, $\Delta T_{fd}$=0 ℃

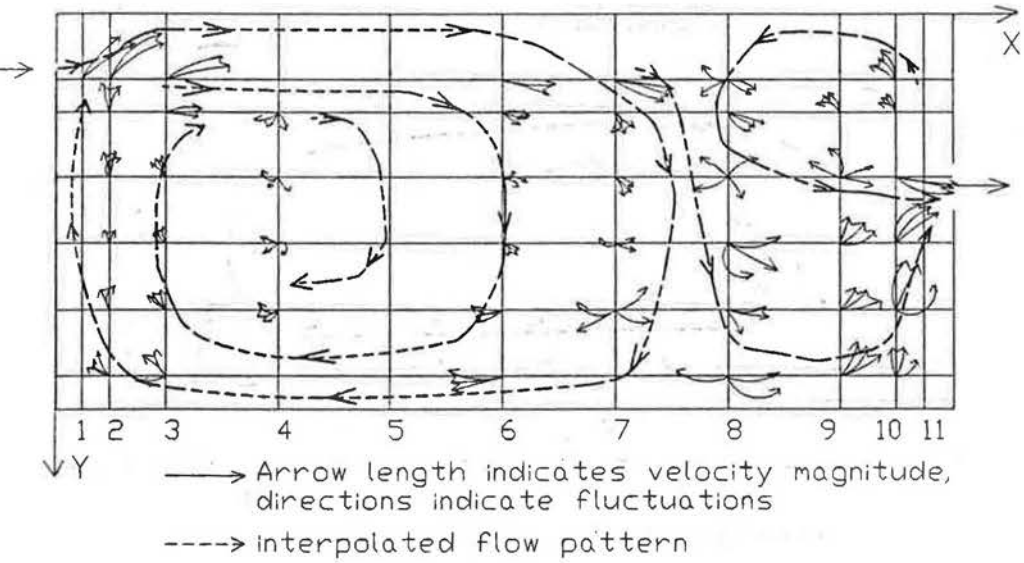


**Figure 6** Flow pattern of test P4: $U_d$=1.78 m/s, $\Delta T_{fd}$=37.4 ℃

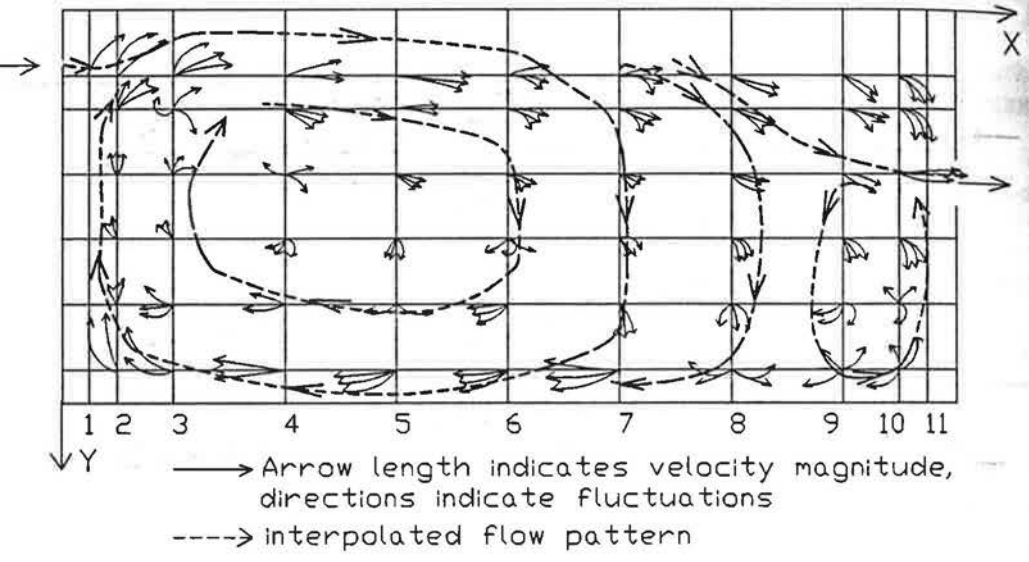


**Figure 7** Flow pattern of test P5: $U_d$=1.78 m/s, $\Delta T_{fd}$=26.6 ℃

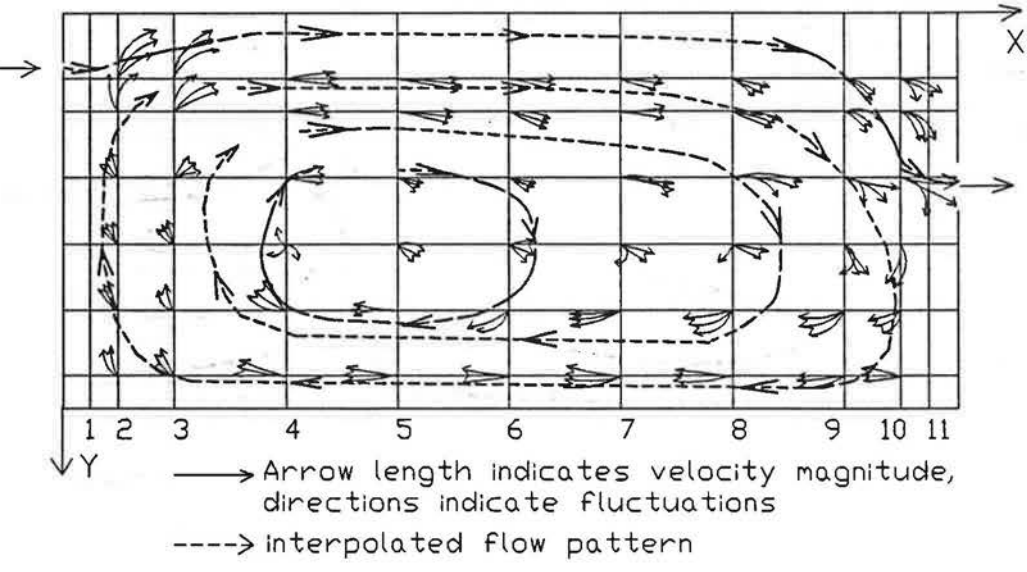


**Figure 8** Flow pattern of test P6: $U_d$=1.78 m/s, $\Delta T_{fd}$=16.4 ℃

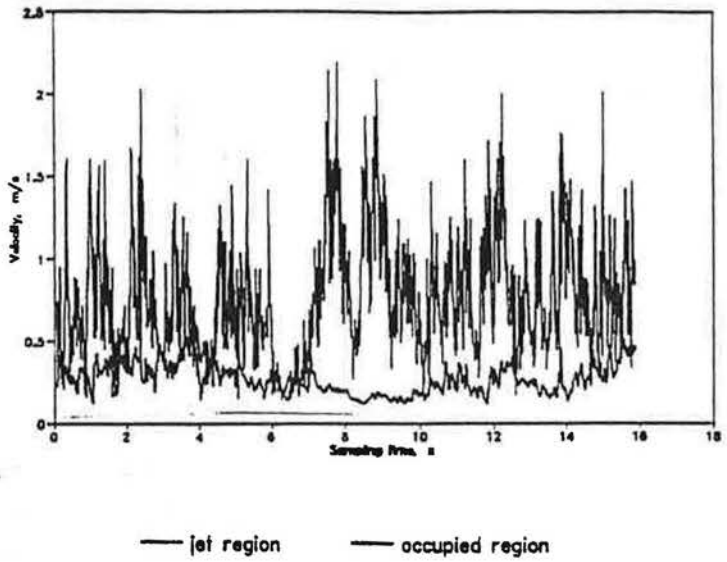


**Figure 9** Sample velocity signals in test P1: $U_d$=2.54 m/s, $\Delta T_{fd}$=0 °C (jet region:x/W=0.125,y/H=0.0521; occupied region:x/W=0.375,y/H=0.6771)

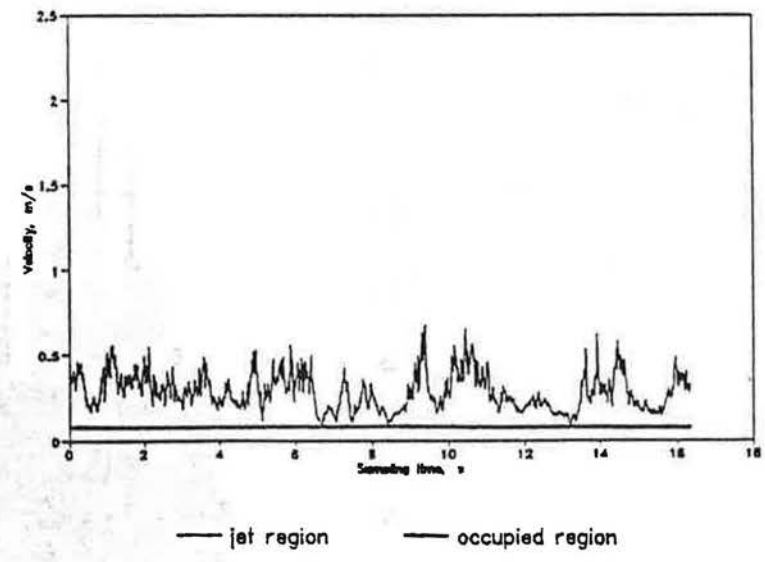


**Figure 10** Sample velocity signals in test P3: $U_d$=0.76 m/s, $\Delta T_{fd}$=0 °C (jet region:x/W=0.125,y/H=0.0521; occupied region:x/W=0.375,y/H=0.6771)

a. jet region:
x/W=0.125, y/H=0.0521

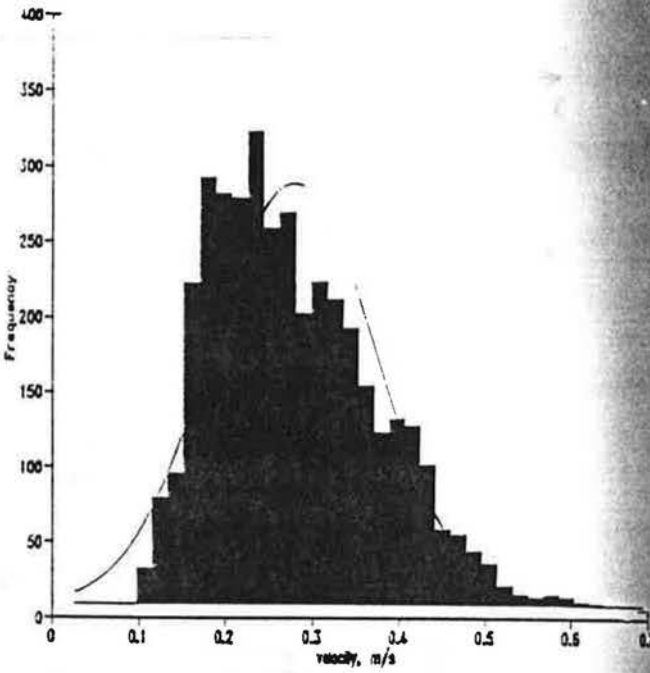


b. occupied region:
x/W=0.375, y/H=0.6771

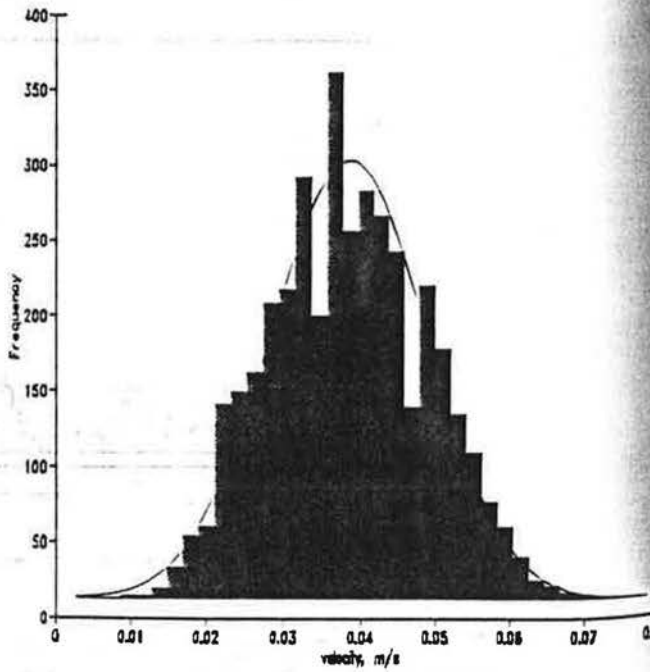


**Figure 11** Histograms of sample velocity signals in test P3:
$U_d$=0.76 m/s, $\Delta T_{fd}$=0 °C

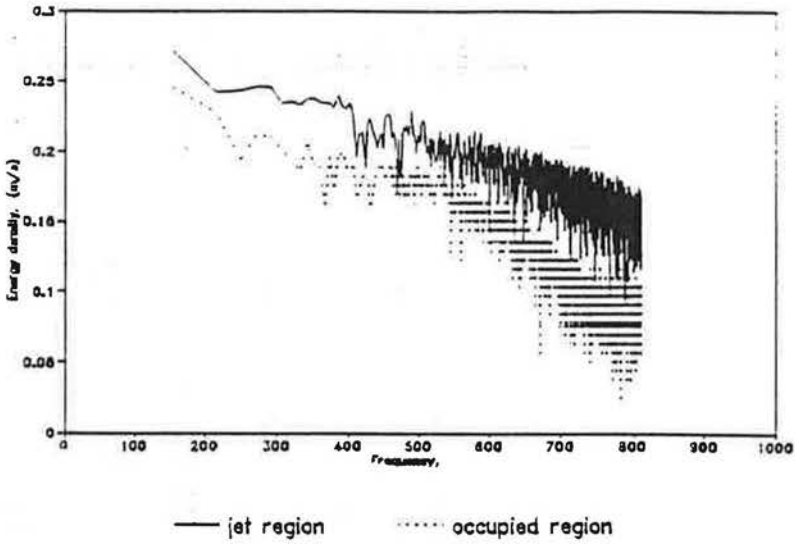


**Figure 12** Energy spectra of velocity in test P1:$U_d$=2.54 m/s,$\Delta T_{fd}$=0 ℃ (jet region:x/W=0.125,y/H=0.0521; occupied region:x/W=0.375,y/H=0.6771)

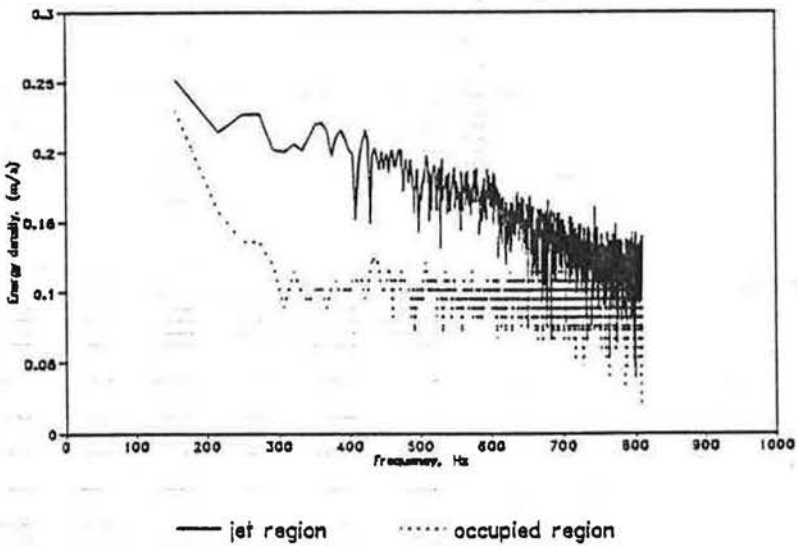


**Figure 13** Energy spectra of velocity in test P3:$U_d$=0.76 m/s,$\Delta T_{fd}$=0 ℃ (jet region:x/W=0.125,y/H=0.0521; occupied region:x/W=0.375,y/H=0.6771)

a. jet region:

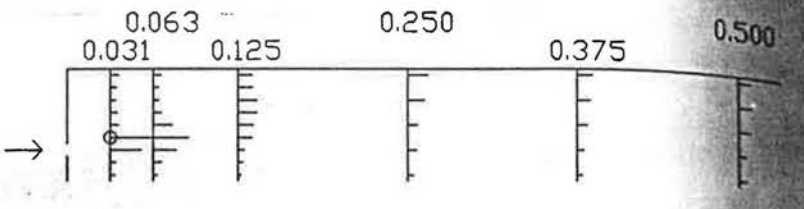


b. entire flow field:

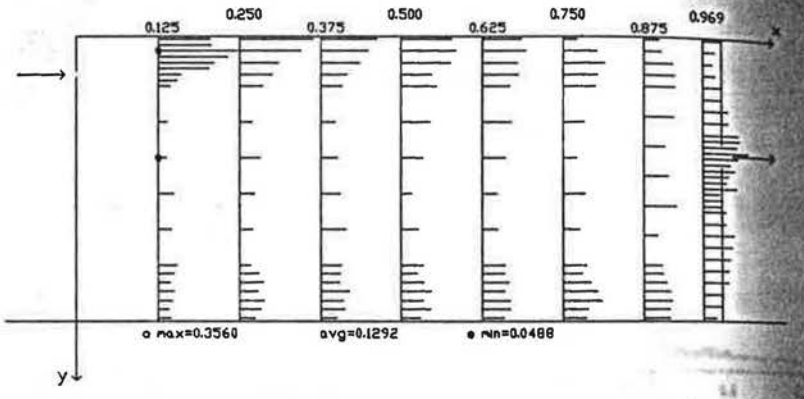


**Figure 14** Distribution of mean velocity ($U/U_d$) for test P6: $U_d$=1.78 m/s, $\Delta T_{fd}$=16.4 °C

a. jet region:

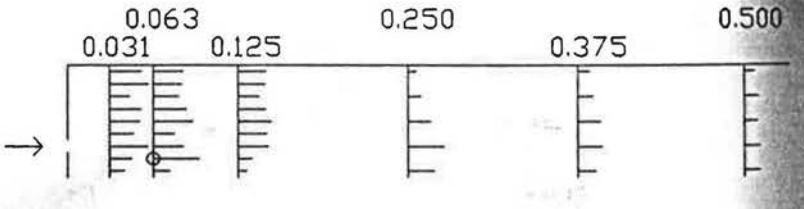


b. entire flow field:

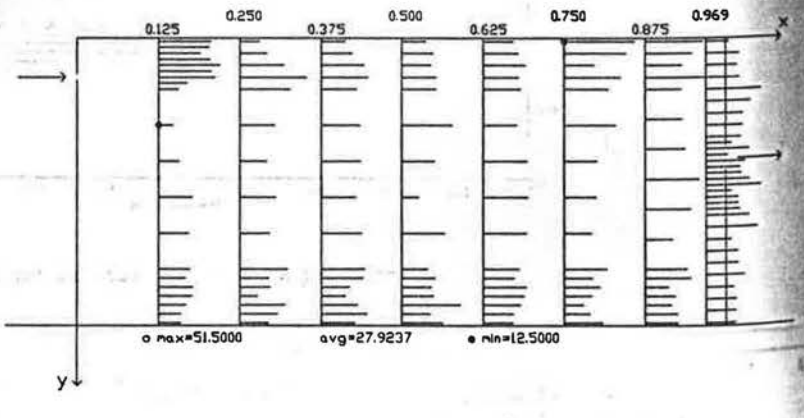


**Figure 15** Distribution of turbulence intensity ($100u'/U$) for test P6: $U_d$=1.78 m/s, $\Delta T_{fd}$=16.4 °C

a. jet region:

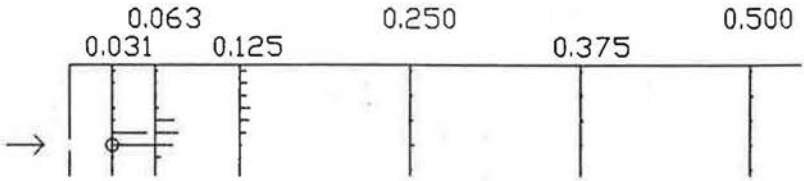


b. entire flow field:

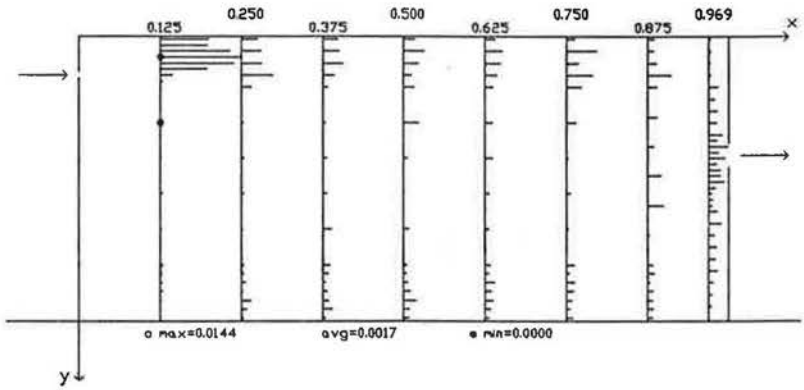


**Figure 16** Distribution of turbulent kinetic energy ($k/0.5U_d^2$) for test P6:$U_d$=1.78 m/s, $\Delta T_{fd}$=16.4 °C

a. jet region:

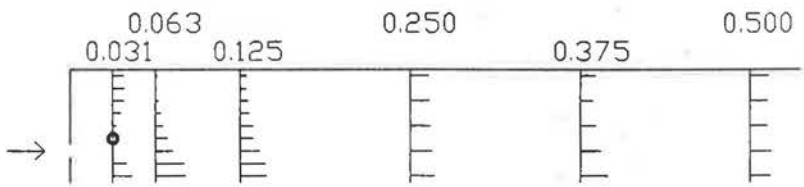


b. entire flow field:

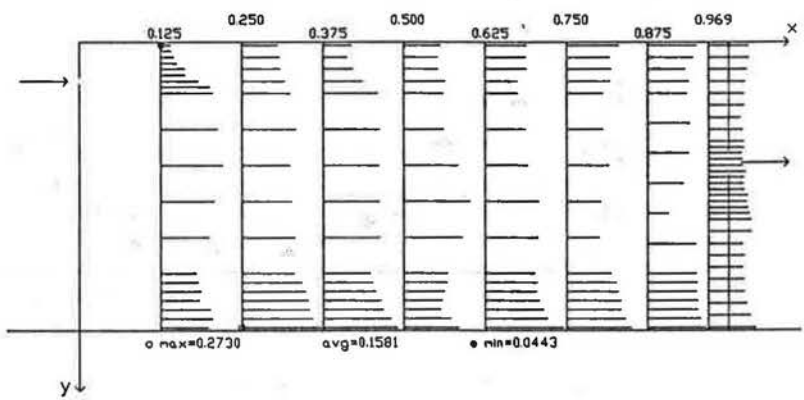


**Figure 17** Distribution of temperature $[(T-T_d)/\Delta T_{fd}]$ for test P6: $U_d$=1.78 m/s, $\Delta T_{fd}$=16.4 °C

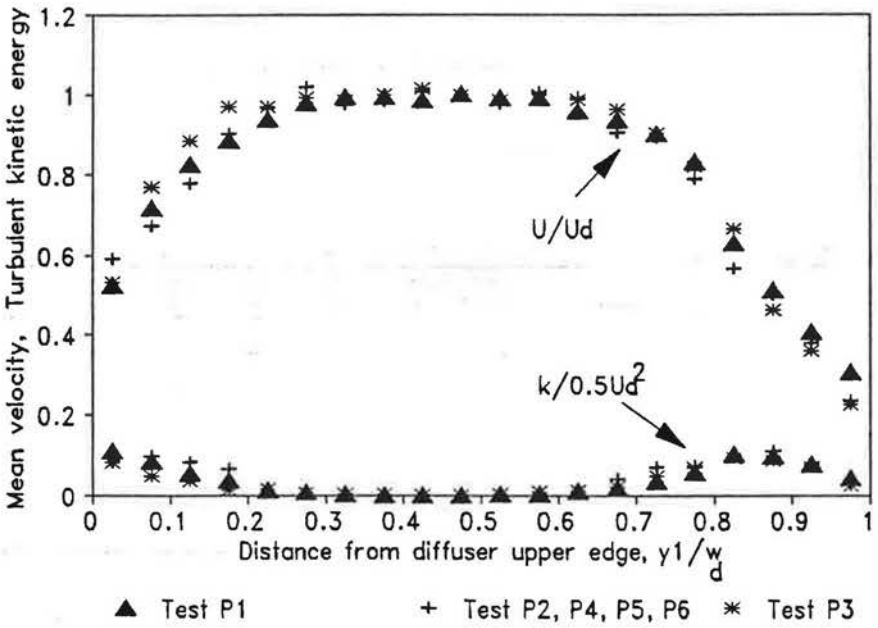


**Figure 18** Profiles of mean velocity and turbulent kinetic energy at the diffuser

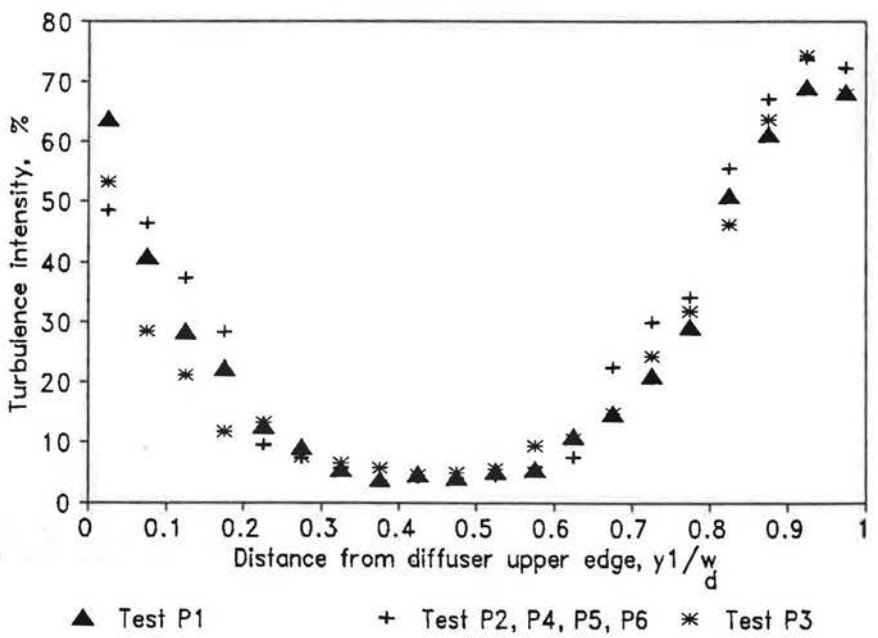


**Figure 19** Profile of turbulence intensity at the diffuser